THE JOURNAL OF BIOLOGICAL CHEMISTRY VOL. 289, NO. 45, pp. 31241–31252, November 7, 2014

Second Transmembrane Helix (M2) and Long Range Coupling in Ca^{2+}-ATPase*

Received for publication, May 27, 2014, and in revised form, September 19, 2014 Published, JBC Papers in Press, September 22, 2014, DOI 10.1074/jbc.M114.584086

Takashi Daiho[1], **Kazuo Yamasaki, Stefania Danko, and Hiroshi Suzuki**

From the Department of Biochemistry, Asahikawa Medical University, Midorigaoka-Higashi, Asahikawa 078-8510, Japan

Background: The catalytic A domain of Ca^{2+}-ATPase moves substantially and connects to distant Ca^{2+} sites through transmembrane helices M1 and M2.
Results: Systematic mutation along M2 profoundly and differentially affects cytoplasmic and luminal gating and catalysis.
Conclusion: M2 plays region- and catalytic step-specific roles in Ca^{2+} transport.
Significance: M2 is a conduit for coupling A domain movements to transport ion gating.

The actuator (A) domain of sarco(endo)plasmic reticulum Ca^{2+}-ATPase not only plays a catalytic role but also undergoes large rotational movements that influence the distant transport sites through connections with transmembrane helices M1 and M2. Here we explore the importance of long helix M2 and its junction with the A domain by disrupting the helix structure and elongating with insertions of five glycine residues. Insertions into the membrane region of M2 and the top junctional segment impair Ca^{2+} transport despite reasonable ATPase activity, indicating that they are uncoupled. These mutants fail to occlude Ca^{2+}. Those at the top segment also exhibited accelerated phosphoenzyme isomerization *E*1P → *E*2P. Insertions into the middle of M2 markedly accelerate *E*2P hydrolysis and cause strong resistance to inhibition by luminal Ca^{2+}. Insertions along almost the entire M2 region inhibit the dephosphorylated enzyme transition *E*2 → *E*1. The results pinpoint which parts of M2 control cytoplasm gating and which are critical for luminal gating at each stage in the transport cycle and suggest that proper gate function requires appropriate interactions, tension, and/or rigidity in the M2 region at appropriate times for coupling with A domain movements and catalysis.

Sarco(endo)plasmic reticulum Ca^{2+}-ATPase (SERCA1a),[2] a representative member of the P-type ion transporting ATPases, catalyzes Ca^{2+} transport coupled with ATP hydrolysis (Fig. 1*A*) (for recent reviews, see Refs. 1–3). The enzyme is activated by the binding of two cytoplasmic Ca^{2+} ions at the cytoplasmic facing high affinity transport sites (*E*2 to *E*1Ca_2 in Fig. 1) and autophosphorylated at Asp^{351} with MgATP to form an ADP-sensitive phosphoenzyme (*E*1P), which reacts with ADP to regenerate ATP in the reverse reaction. Upon *E*1P formation, the two bound Ca^{2+} are occluded in the transport sites (*E*1PCa_2). The subsequent isomeric transition to the ADP-insensitive *E*2P form results in rearrangements of the Ca^{2+} binding sites to deocclude Ca^{2+}, open the release path, and reduce the affinity, thus releasing Ca^{2+} into the lumen. Finally, the Asp^{351}-acylphosphate in *E*2P is hydrolyzed to form a Ca^{2+}-unbound inactive *E*2 state. During the hydrolysis, the Ca^{2+} release path is closed, thereby preventing possible luminal Ca^{2+} access to the transport sites and Ca^{2+} leakage.

In the transport cycle, the three cytoplasmic domains N, P, and A undergo large movements and change their organizational state, a repositioning that is coupled to rearrangements in transmembrane helices and thereby changes in the transport sites (1–15). Most remarkable is the motion of the A domain, which functions in cytoplasmic and luminal gating to regulate Ca^{2+} binding and release as well as the *E*2P hydrolysis. The critical importance of the M1/M2 segment, which forms a V-shaped rigid body connected with the A domain, for luminal gating is nicely demonstrated by the crystal structures of catalytic intermediates with bound substrate analogs (9, 11). The long helix M2 connects directly with the A domain at their junction (A/M2-junction) and moves largely together with the A domain and also changes its secondary structure, unwinding/rewinding with consequent length changes, during the Ca^{2+} transport cycle (Fig. 1*A*). Notably, a long helix structure of M2 and the A domain motions are common features in P-type ion-transporting ATPases (16–20). With the Ca^{2+}-ATPase, we previously demonstrated (21, 22) that Tyr^{122} and Leu^{119} at the A/M2-junction and the top part of M2 (M2top) form a hydrophobic interaction network, which includes a Tyr^{122}-hydrophobic cluster (an interaction with the P domain (Val^{706}/Val^{726}), with the loop connecting the A domain and M3 (A/M3-linker, Ile^{232}), and with the A domain (Ile^{179}/Leu^{180}) in *E*2P) and that this formation is critical for stabilizing *E*2P structure with the luminal gate open and the potential for hydrolytic activity at the catalytic site. However, the importance of other M2 regions as well as of the long M2 helix structure itself has not yet been fully explored.

* This work was supported by a Grant-in-Aid for Scientific Research C (to T. D.) and B (to H. S.) from the Ministry of Education, Culture, Sports, Science, and Technology of Japan.

[1] To whom correspondence should be addressed: Dept. of Biochemistry, Asahikawa Medical University, Midorigaoka-Higashi, Asahikawa, 078-8510, Japan. Tel.: 81-166-68-2353; Fax: 81-166-68-2359; E-mail: daiho@asahikawa-med.ac.jp.

[2] The abbreviations used are: SERCA1a, adult fast twitch skeletal muscle sarcoplasmic reticulum Ca^{2+}-ATPase; A, N, and P domain, actuator, nucleotide binding, and phosphorylation domain, respectively; *E*P, phosphoenzyme; *E*1P, ADP-sensitive phosphoenzyme; *E*2P, ADP-insensitive phosphoenzyme; *E*2∼$P^{‡}$, transition state of ADP-insensitive phosphoenzyme hydrolysis; *E*1PCa_2, ADP-sensitive phosphoenzyme with occluded Ca^{2+}; *E*2PCa_2, ADP-insensitive phosphoenzyme with occluded Ca^{2+}; TG, thapsigargin; aa, amino acid(s); PDB, Protein Data Bank; 5Gi, insertion of five glycine residues.

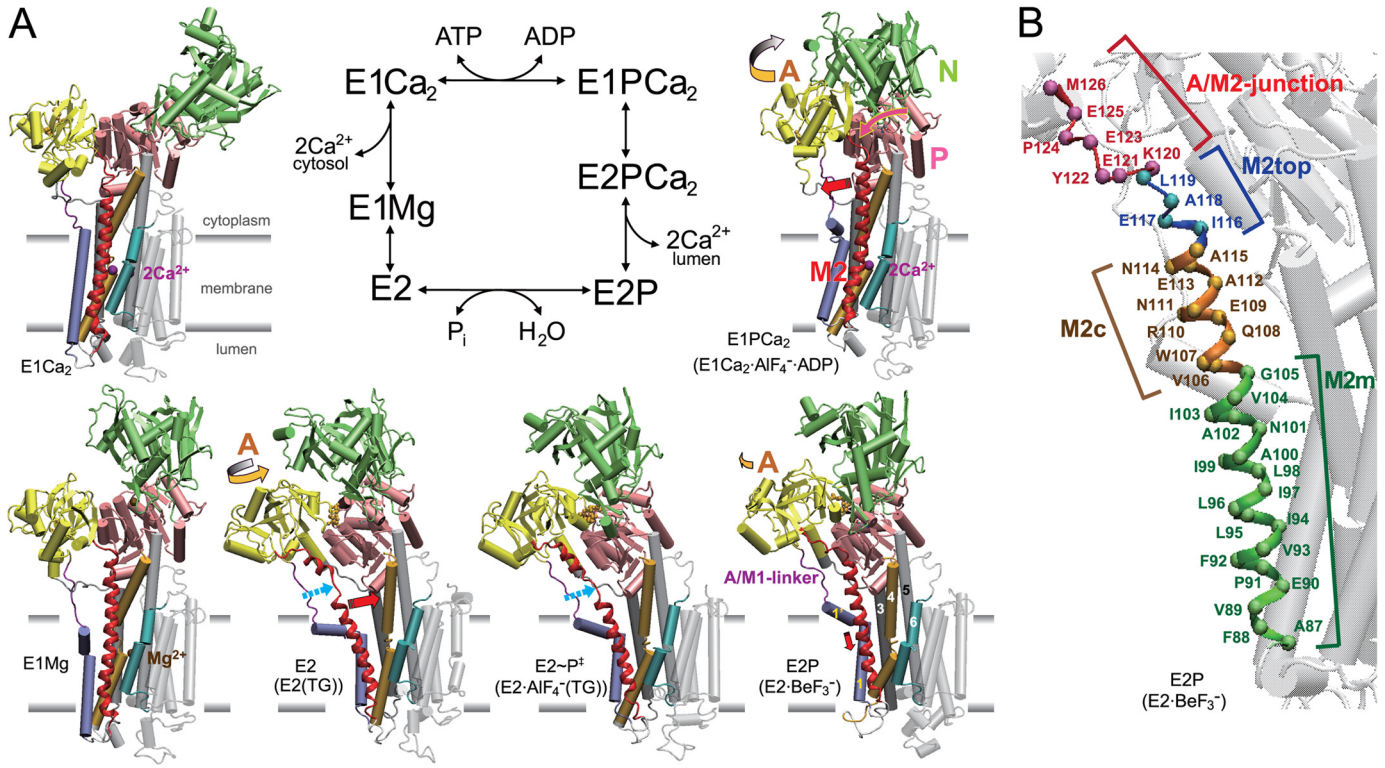

FIGURE 1. **Reaction cycle and structural changes of Ca^{2+}-ATPase.** *A*, the structural changes are modeled on the crystal structures $E1Ca_2{\cdot}AlF_4^-{\cdot}ADP$ as the $E1{\sim}P{\cdot}ADP{\cdot}Ca_2$ analog (PDB code 1T5T (10)), $E2{\cdot}BeF_3^-$ as the *E*2P ground state analog (7) (PDB code 2ZBE (11)), $E2{\cdot}AlF_4^-$(TG) as the transition state analog for *E*2P hydrolysis (7) (PDB 2ZBG (11)), *E*2(TG) as the *E*2 state fixed with thapsigargin (PDB 1IWO (6)), $E1Mg^{2+}$ (PDB 3W5A (14)), and $E1Ca_2$ (PDB 1SU4 (4)). The structures are aligned with the static M8–M10 helices. The N, P, and A domains and M1–M6 helices are *colored* as indicated. The approximate position of the membrane is shown by *gray lines*. The binding sites for two Ca^{2+} (*purple spheres*) consist of residues on M4, M5, M6, and M8. The *yellow*, *pink*, and *red arrows* indicate the approximate motions of the A and P domains and M2 (depicted in *red*), respectively, to the next structural state during the *EP* processing (isomerization and hydrolysis) and the $E2 \rightarrow E1$ transition. The *broken light blue arrow* indicates the unwound M2 part. *B*, the regions of M2 are named as M2m (transmembrane part), M2c (cytoplasmic part), M2top (top part), and A/M2-junction (junction with the A domain) and indicated with *different colors* on the α-carbon of residues.

In this study, we focus on each region of the long helix M2: transmembrane M2m, cytoplasmic M2c, M2top, and A/M2-junction (Fig. 1*B*). We explored their roles and the functional significance of the changes in secondary structure and length for the coupling of the different conformational steps that are required to efficiently convert the chemical energy of ATP hydrolysis into the changes in accessibility, orientation, and affinity of the Ca^{2+} binding transport sites.

In extensive preliminary experiments, we first introduced a series of mutations at various positions throughout: insertions of 1–5 glycine residues, deletions of 1–4 successive residues, glycine substitutions of 2 or 3 successive residues, and some specific substitutions. In detailed kinetic analyses, we found that results were most clear with the insertions of five glycine residues (5Gis), which disrupt the helix structure and elongates, showing profound region-specific and catalytic step-specific effects. Therefore, we present here the results obtained for the 5Gi insertions. Our results demonstrate that different parts of the A/M2 link play a critical role in synchronizing gating of the two Ca^{2+} at the transport sites on both sides of the membrane, and each is therefore part of the mechanism for coupling catalytic and transport site structural events. M2 and its connection with the A domain have a role distinct from that of the A/M1′-linker loop (23–25), although both are needed to coordinate coupling.

EXPERIMENTAL PROCEDURES

Mutagenesis and Expression—The pMT2 expression vector (26) carrying rabbit SERCA1a cDNA with a desired mutation was constructed as described previously (24). Transfection of pMT2 DNA into COS-1 cells and preparation of microsomes from the cells were performed as described (27). The amount of expressed SERCA1a was quantified by a sandwich enzyme-linked immunosorbent assay (28).

Ca^{2+}-ATPase Activity and Ca^{2+} Transport Activity—Activities of expressed SERCA1a were obtained essentially as described previously (29). The rate of ATP hydrolysis was determined at 25 °C in a mixture containing 1–5 μg of microsomal protein, 0.1 mM [γ-^{32}P]ATP, 0.1 M KCl, 7 mM $MgCl_2$, 0.1 mM $CaCl_2$, 5 mM potassium oxalate, and 50 mM MOPS/Tris (pH 7.0). The Ca^{2+}-ATPase activity of expressed SERCA1a was obtained by subtracting the ATPase activity determined in the presence of 1 μM thapsigargin (TG), a specific inhibitor of SERCA, with conditions otherwise as above. The rate of Ca^{2+} transport was determined with $^{45}Ca^{2+}$ and nonradioactive ATP, otherwise as above. The Ca^{2+} transport activity of expressed SERCA1a was obtained by subtracting the activity determined in the presence of 1 μM TG, with conditions otherwise as above.

Formation and Hydrolysis of EP—Phosphorylation of SERCA1a in microsomes with [γ-^{32}P]ATP or $^{32}P_i$ and dephos-

phorylation of ^{32}P-labeled SERCA1a were performed under conditions described in the legends to Figs. 4–9. The reaction was quenched with ice-cold trichloroacetic acid containing P_i. Precipitated proteins were separated by 5% SDS-PAGE at pH 6.0 according to Weber and Osborn (30). The radioactivity associated with the separated Ca^{2+}-ATPase was quantified by digital autoradiography as described (31). The amount of *E*P in expressed SERCA1a was obtained by subtracting the background radioactivity determined in the presence of 1 μM TG, with conditions otherwise as above.

Ca^{2+} Occlusion in EP—Microsomes were phosphorylated for 1 min at 0 °C in a mixture containing 1–5 μg of microsomal protein, 5 μM ATP, 0.1 M KCl, 7 mM $MgCl_2$, 10 μM $^{45}CaCl_2$, 1 μM A23187, and 50 mM MOPS/Tris (pH 7.0) and immediately filtered through a 0.45-μm nitrocellulose membrane filter (Millipore). The filter was washed extensively with a washing solution (1 mM EGTA, 0.1 M KCl, 7 mM $MgCl_2$, and 20 mM MOPS/Tris (pH 7.0)), and $^{45}Ca^{2+}$ remaining on the filter was quantified as described (24). The amount of Ca^{2+} occluded at the transport sites of *E*P in the expressed SERCA1a was obtained by subtracting the amount of nonspecific Ca^{2+}-binding determined in the presence of 1 μM TG, with conditions otherwise as above. The amount of *E*P formed was determined with nonradioactive Ca^{2+} and [γ-^{32}P]ATP under otherwise the same conditions as above by membrane filtration, and the radioactivity remaining on the filter was quantified.

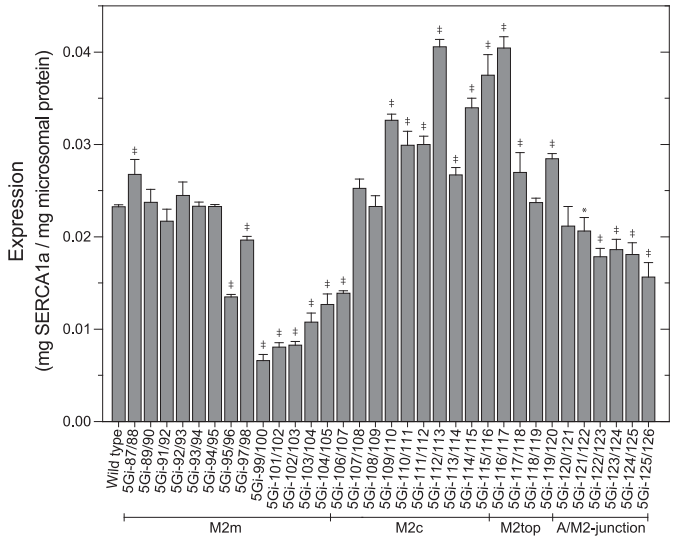

FIGURE 2. **Expression levels.** The expression levels of wild-type and 5Gi mutant SERCA1a in the microsomes prepared from COS-1 cells were determined and shown as values relative to the total amount of protein in the microsomes. Statistical significance compared with the wild type is shown as follows: *, $p < 0.05$; ‡, $p < 0.01$. *Error bars*, S.D.

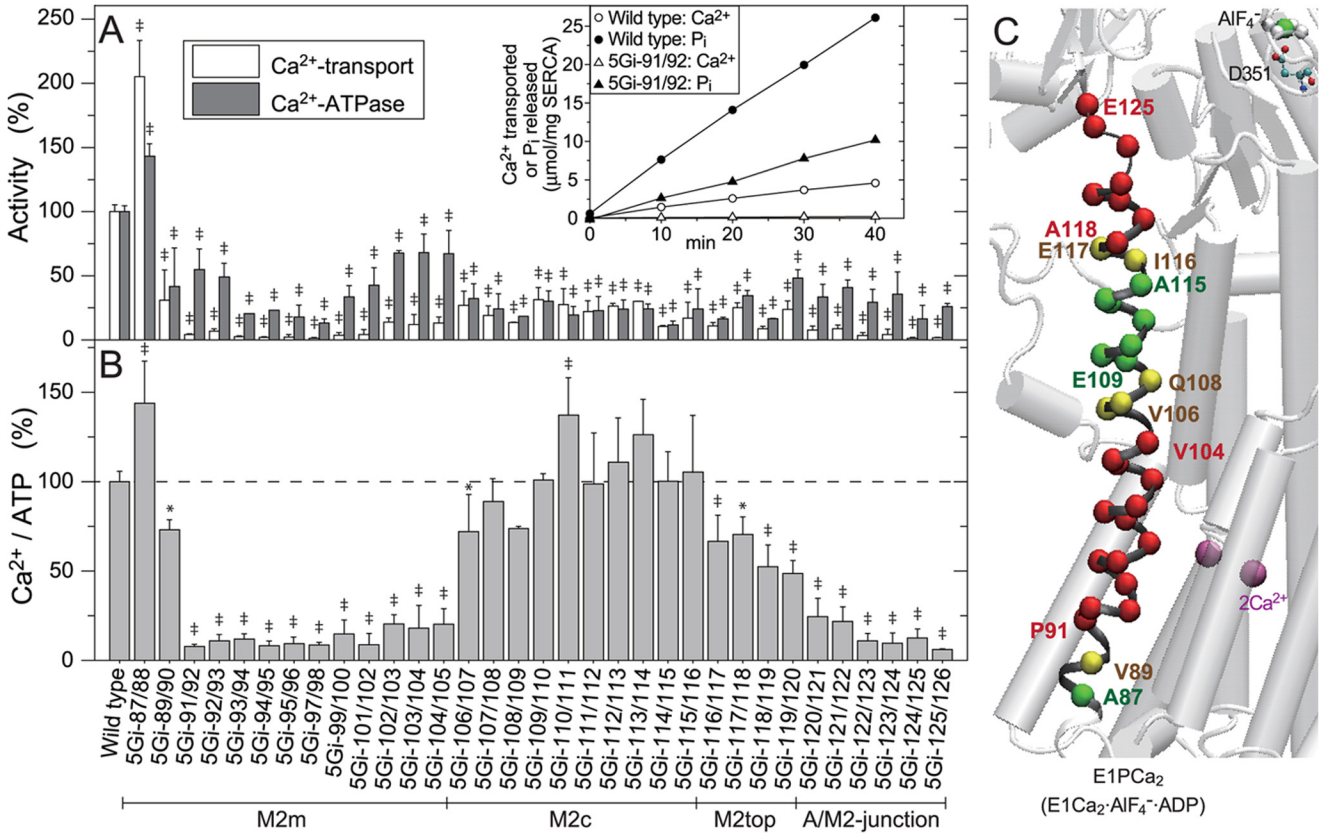

FIGURE 3. **Ca^{2+}-ATPase and oxalate-dependent Ca^{2+} transport activities.** *A*, the specific activities of the expressed SERCA1a 5Gi mutants were determined and shown as values relative to the respective wild-type activities (ATP hydrolysis, 0.594 ± 0.028 μmol of P_i/min/mg of SERCA1a protein ($n = 5$); oxalate-dependent Ca^{2+} transport, 0.116 ± 0.006 μmol Ca^{2+}/min/mg SERCA1a protein ($n = 5$); very similar to the values obtained by our group and other groups under optimum conditions with the microsomes prepared from the COS cells (*e.g.* see Refs. 29, 47–49)). Typical time courses of P_i liberation and Ca^{2+} accumulation in the wild type and mutant 5Gi-91/92 are shown in the *inset*. *B*, the coupling ratio (*i.e.* Ca^{2+} transport activity per Ca^{2+}-ATPase activity (*Ca^{2+}/ATP*)), is shown as a percentage of the wild-type ratio. In *A* and *B*, statistical significance compared with the respective wild-type value is shown; *, $p < 0.05$; ‡, $p < 0.01$. *C*, the mutational effects of residues in *B* are visualized with α-carbon coloring on M2; *green*, *Ca^{2+}/ATP* higher than 80% of the wild type (coupled transport); *yellow*, 80 to 60% (slightly uncoupled); *red*, less than 60% (severely uncoupled). *Error bars*, S.D.

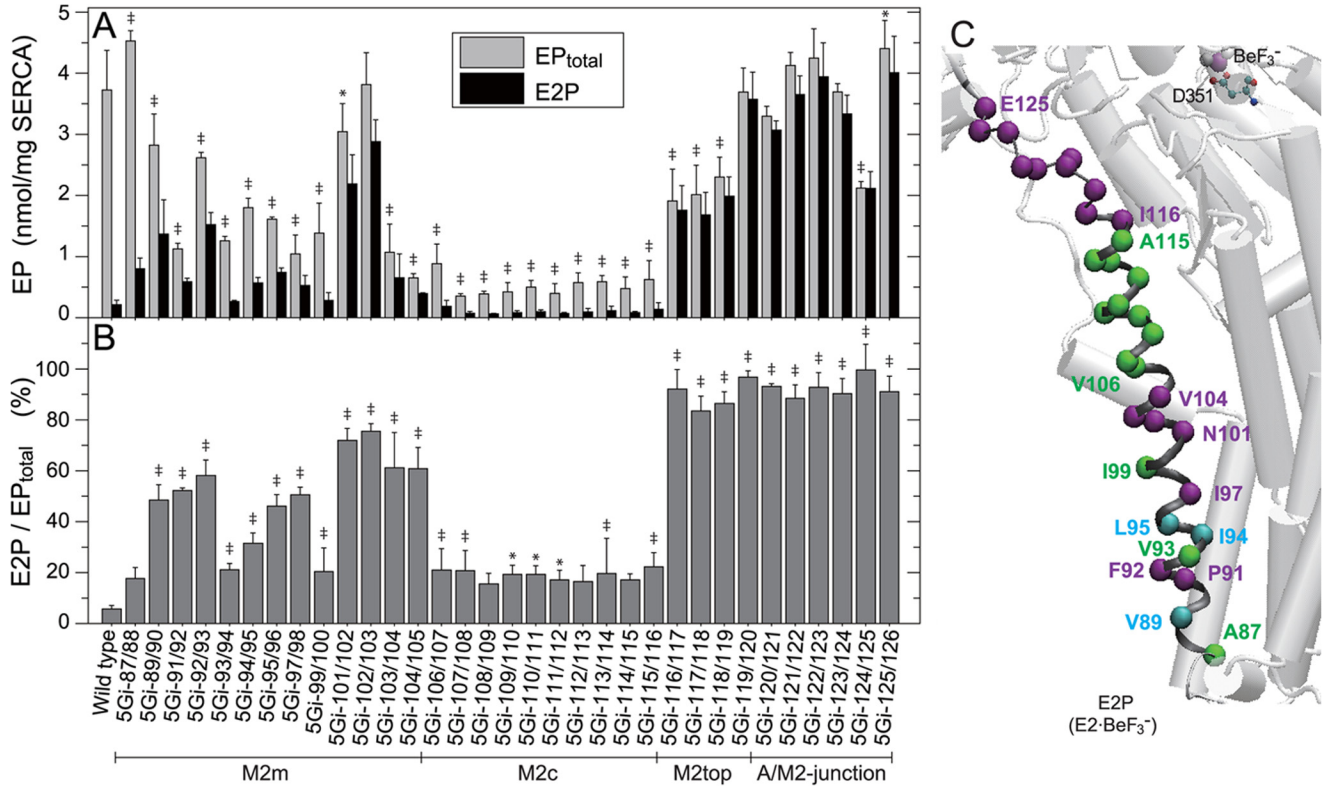

FIGURE 4. **Total amount of *EP* (EP_{total}) at steady state and *E2P* fraction.** *A*, microsomes expressing wild type or the 5Gi mutant were phosphorylated with [γ-^{32}P]ATP at 0 °C for 1 min in 50 μl of a mixture containing 1–5 μg of microsomal protein, 10 μM [γ-^{32}P]ATP, 1 μM A23187, 0.1 M KCl, 7 mM $MgCl_2$, 0.1 mM $CaCl_2$, and 50 mM MOPS/Tris (pH 7.0). The EP_{total} formed (*gray bars*) was determined by acid quenching. For determination of *E2P* (*closed bars*), an equal volume of a mixture containing 2 mM ADP, 1 μM A23187, 0.1 M KCl, 7 mM $MgCl_2$, 10 mM EGTA, and 50 mM MOPS/Tris (pH 7.0) was added to the above phosphorylation mixture, and the reaction was quenched at 1 s after the ADP addition. ADP-sensitive *EP* (*E1P*) disappeared entirely within 1 s after the ADP addition. *B*, the *E2P* fraction in EP_{total} (*E1P* plus *E2P*) is shown. Statistical significance compared with the wild type is shown for EP_{total} (*A*) and for *E2P*/EP_{total} (*B*): *, $p < 0.05$; ‡, $p < 0.01$. *C*, the mutation effects of residues in *B* are visualized with α-carbon coloring: *green*, *E2P*/EP_{total} less than 30% (almost no or slight *E2P* increase); *light blue*, 30–50% (moderate increase); *purple*, higher than 50% (marked increase). *Error bars*, S.D.

Miscellaneous—Protein concentration was determined by the method of Lowry *et al.* (32) with bovine serum albumin as a standard. Data were analyzed by nonlinear regression using the program Origin (MicroCal Software, Inc., Northampton, MA). Three-dimensional models of the enzyme were reproduced by the program VMD (33). The data represent the mean ± S.D. for 2–6 independent experiments (or 8–18 experiments in Fig. 6). Statistical analysis was performed by one-way analysis of variance with Dunnett's post hoc test using SPSS software version 22.

RESULTS

Protein Expression Level—For understanding possible structural roles of each of the M2 regions and the functional significance of its helix structure and changes during the transport cycle (unwinding/elongation) (Fig. 1), we introduced 5Gis throughout M2 and performed functional analyses. We first determined the expression levels of the wild type and mutants in the microsomes prepared from COS-1 cells (Fig. 2). The expression level of wild-type SERCA1a in the microsomes is ~2% of total microsomal protein. Those of the 5Gi mutants are comparable, although a few show a level that is somewhat reduced but still high enough to perform all functional analyses.

ATP Hydrolysis, Ca^{2+} Transport, and Their Coupling—First, we explored possible effects of 5Gi mutations on the overall transport cycle. Fig. 3*A* shows the specific Ca^{2+}-ATPase and oxalate-dependent Ca^{2+} transport activities of SERCA1a mutants and wild type at 10 μM Ca^{2+} in the presence of 5 mM oxalate. Here, the activities were determined during the linear part of P_i liberation and Ca^{2+} transport (*inset*) and defined as the fraction that is sensitive to inhibition by 1 μM TG, a highly specific and subnanomolar affinity SERCA inhibitor (34). We first confirmed that the mutants all retain TG sensitivity by observing that TG (1 μM) completely inhibits *E*P formation from [γ-^{32}P]ATP in 10 μM Ca^{2+}, conditions essentially the same as the activity measurements. We found that TG reduces the *E*P value in all cases to a background radioactivity level as in the wild type (*i.e.* less than 1% of the maximum *E*P level). The background radioactivity level is actually the same as that obtained in the absence of Ca^{2+} without TG.

Most insertions reduce both activities (Fig. 3*A*). Importantly, some mutations at specific regions decrease Ca^{2+} transport/ATPase activity ratios (Ca^{2+}/ATP, Fig. 3*B*). The insertions in M2m and those in the A/M2-junction cause severe uncoupling (*i.e.* almost no Ca^{2+} transport despite fair ATP hydrolysis). This contrasts with mutations at M2c, which result in normal coupling. At M2top (aa 116–119), uncoupling increases with proximity of the 5Gi insertions to the A/M2-junction.

EP Formation from ATP and E1P → E2P Isomerization—We then analyzed each of the steps and intermediates in the Ca^{2+} transport cycle. In Figs. 4–7, we assessed possible effects of 5Gi

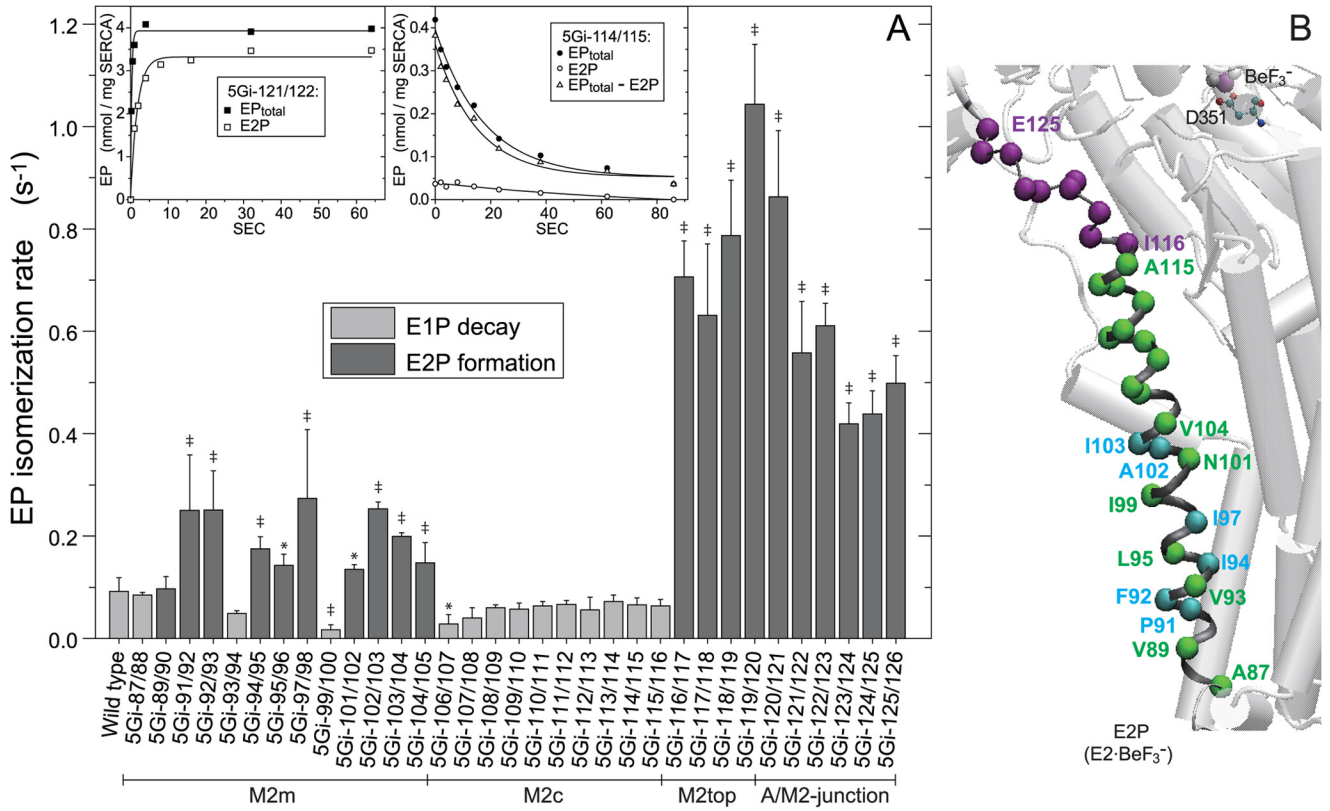

FIGURE 5. ***EP* isomerization rate.** *A*, for the wild type and mutants that accumulate mostly *E*1P at steady state (*E*2P less than 30% of EP_{total}; *cf.* Fig. 4), the *E*1P to *E*2P isomerization rate was determined by *E*1P decay kinetics, which represent the rate-limiting *E*1P to *E*2P isomerization (mutant 5Gi-114/115 (*right inset*) is a typical example). Here, the Ca^{2+}-ATPase was first phosphorylated with [γ-^{32}P]ATP at 0 °C for 1 min as in Fig. 4; phosphorylation was terminated by Ca^{2+} removal and the addition of an equal volume of a buffer containing 10 mM EGTA, 0.1 M KCl, 7 mM $MgCl_2$, and 50 mM MOPS/Tris (pH 7.0) at 0 °C; and the amounts of EP_{total} and *E*2P were determined at the indicated times. The amount of *E*1P was calculated by subtracting *E*2P from EP_{total} ($EP_{total} - E2P$). *Solid lines* show the least squares fit to a single exponential, and the *E*1P decay rates thus obtained are shown in the *main panel* (*light gray bar*). For the mutants that accumulate *E*2P more than 30% of EP_{total} (*cf.* Fig. 4), the *EP* isomerization rate was determined as the apparent rate of *E*2P formation from *E*1P to reach steady state as follows (mutant 5Gi-121/122 (*left inset*) is a typical example). Here, the Ca^{2+}-ATPase was phosphorylated for the indicated periods after ATP addition, and the amounts of EP_{total} and *E*2P were determined; otherwise, conditions were as described above. The formation of *EP* (EP_{total}, representing $E1PCa_2$ formation from $E1Ca_2$) was very fast (reaching a steady state within ~1 s) and was followed by *E*2P formation from $E1PCa_2$. *Solid lines* show the least squares fit to a single exponential, and the apparent rates of *E*2P formation are shown in the *main panel* (*dark gray bar*). Statistical significance compared with the wild type is shown: *, $p < 0.05$; ‡, $p < 0.01$. *B*, the mutation effects of residues in *A* are visualized with α-carbon *coloring*: *green*, transition rate less than 0.15 s^{-1} (almost no effect or only a slight effect); *light blue*, 0.15–0.3 s^{-1} (moderate acceleration); *purple*, higher than 0.3 s^{-1} (marked acceleration). *Error bars*, S.D.

mutations on the properties of the phosphorylated intermediates *E*1P (occludes Ca^{2+} at the transport sites) and *E*2P (releases Ca^{2+} into the lumen). We first determined in Fig. 4 the total amount of *EP* (EP_{total}, sum of *E*1P and *E*2P) and the *E*2P fraction at steady state. The analysis was made in the presence of K^+, which strongly accelerates hydrolysis of *E*2P and therefore suppresses its accumulation in the wild type (35). The 5Gi insertions at aa 103–115 in M2m to M2c markedly decrease EP_{total} (Fig. 4*A*). The decrease seems to correlate well with Ca^{2+} insensitivity of the *EP* hydrolysis rate in these mutants (see Fig. 7). It is also possible that a very rapid *E*2P hydrolysis and a very slow $E2 \rightarrow E1$ transition in these mutants (*cf.* Figs. 7 and 8) may contribute to the decrease in EP_{total}.

Otherwise, 5Gi mutants in M2c are largely wild type-like; *E*2P accumulation, the *E*1P to *E*2P isomerization rate (Figs. 4*B* and 5), and coupled Ca^{2+} transport are unremarkable. At M2m, *E*2P accumulation is considerably higher in some 5Gi mutants (5Gi-91/92, 5Gi-92/93, 5Gi-97/98, and 5Gi-101/102 to 5Gi-104/105) (Fig. 4*B*); *EP* isomerization is slightly faster than in the wild type (Fig. 5); and coupling in Ca^{2+} transport is substantially reduced as noted above.

At the M2top and A/M2-junction (aa 116–119 and 120–126), almost all EP_{total} is *E*2P in the 5Gi mutants despite the presence of K^+ (Fig. 4). In these mutants, *EP* isomerization is markedly accelerated (Fig. 5), and *E*2P hydrolysis is strongly retarded (as shown in Fig. 7), consistent with the dominant *E*2P accumulation. Ca^{2+} transport is substantially uncoupled from ATPase activity as noted above.

Ca^{2+} Occlusion in EP—In Fig. 6, the amount of $^{45}Ca^{2+}$ occluded in *EP* was determined after *EP* formation under otherwise the same conditions as in Fig. 4. In the wild type, approximately two Ca^{2+} ions were occluded in EP_{total} (comprising mostly *E*1P; Fig. 4*B*), in agreement with established mechanisms. 5Gi mutants at the luminal end of M2m (5Gi-87/88 and 5Gi-89/90) and those at the M2c region (aa 106–115) occluded approximately two Ca^{2+} in *E*1P (*cf.* Fig. 4*B*), which fits with their coupled Ca^{2+} transport although turnover is severely inhibited.

In contrast, in 5Gi mutants at M2m aa 91–105, all of which show severe uncoupling (*cf.* Fig. 3*B*), no Ca^{2+} is occluded despite reasonable *E*1P accumulation. Bound Ca^{2+} must escape from the *E*1P state, probably to the cytoplasmic side, to account

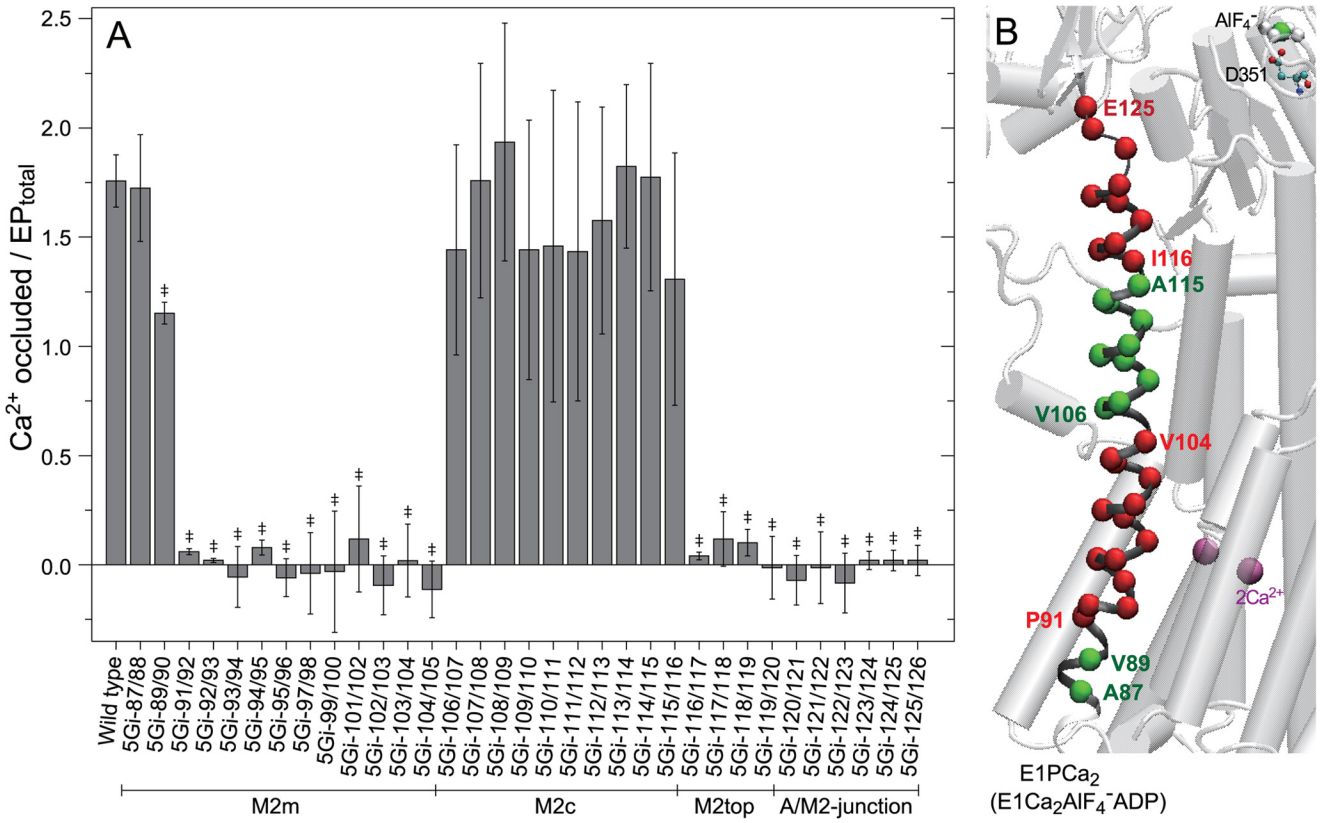

FIGURE 6. **Ca^{2+} occlusion in *EP*.** *A*, phosphorylation was performed with ATP in 10 μM $^{45}Ca^{2+}$; otherwise conditions were as in Fig. 4. The amount of Ca^{2+} occluded was determined as described under "Experimental Procedures" and is shown as the value relative to EP_{total} (mean ± S.D. (n = 8–18)). Statistical significance compared with the wild type is shown: *, $p < 0.05$; ‡, $p < 0.01$. *B*, the mutation effects of residues in *A* are visualized with α-carbon *coloring*; *green*, Ca^{2+} occluded/EP_{total} above 1.0; *red*, below 0.15. *Error bars*, S.D.

for the uncoupling. For 5Gi mutants at M2top to the A/M2-junction region (aa 116–126), we also did not observe Ca^{2+} occlusion, but in this case, it is rather due to the dominant *E*2P accumulation and very rapid *E*P isomerization (Figs. 4 and 5). Nevertheless, in the uncoupled mutants, especially at the A/M2-junction, the Ca^{2+} must escape from *E*1P or during *E*P isomerization to the cytoplasmic side, showing the critical importance of this junctional region to keep the gate closed. The increased severity of uncoupling as the 5Gi insertions approach the A/M2-junction emphasizes its importance in coupling. In summary, 5Gi insertions in the central section of M2 have little effect on cytoplasmic gating, whereas those on either side block gate closure, although mutations at M2top (*i.e.* at the border region between M2c and A/M2-junction) exhibit mixed properties.

E2P Hydrolysis—Then we assessed possible effects of 5Gi mutations on the *E*2P hydrolysis rate and luminal Ca^{2+}-induced back-inhibition of hydrolysis that reflect luminal gate closure during hydrolysis. The closure prevents luminal Ca^{2+} access to the transport sites and leakage. Here we determined the *E*2P hydrolysis rate directly by first phosphorylating the enzyme with $^{32}P_i$ in the absence of Ca^{2+} and K^+ and the presence of 35% (v/v) Me_2SO, which strongly favors *E*2P formation in the reverse reaction (36), and then diluting the phosphorylated protein with a large volume of nonradioactive P_i and K^+ without Ca^{2+} (*open bars* in Fig. 7). In regions M2m (aa 87–102), M2top (aa 116–119), and the A/M2-junction (aa 120–126), the 5Gi insertions strongly retard *E*2P hydrolysis. In contrast, at the top of M2m (aa 103–105) and the entire M2c region (aa 106–115), the insertions stimulate hydrolysis 3–10-fold.

Importantly, those mutants showing marked acceleration of *E*2P hydrolysis are insensitive to luminal Ca^{2+}-induced back-inhibition. Here, the *E*2P hydrolysis rate was determined in the presence of 3 (*gray bars*) or 20 mM (*black bars*) Ca^{2+} and ionophore A23187. In the wild type, *E*2P hydrolysis is completely blocked by 3 mM Ca^{2+} due to Ca^{2+} binding to the open luminally oriented transport sites (open luminal gate) in *E*2P, in agreement with previous findings. Thus, accessibility to the Ca^{2+} sites from the luminal side in *E*2P, reflecting open gate status, can be assessed by the back-inhibition (22, 24, 37–42). All of the mutants with accelerated *E*2P hydrolysis are resistant against inhibition by Ca^{2+} even at 20 mM. The luminal gate is tightly closed, preventing access of Ca^{2+} to its binding site, or Ca^{2+} binding is possibly no longer coupled to a large change in the rate of hydrolysis. The results, either way, indicate the importance of the M2c region for coupling catalysis and luminal gate closure during *E*2P hydrolysis. Notable also, 5Gi mutants at aa 95–101 with retarded hydrolysis exhibit partial resistance to inhibition by luminal Ca^{2+} although less than those at aa 103–115.

E2 → E1 Transition—After *E*2P hydrolysis, the enzyme in the inactive *E*2 state is reactivated for the next transport cycle by two Ca^{2+} binding from the cytoplasmic side to the high affinity transport sites forming $E1Ca_2$. In this activation, the *E*2 state is

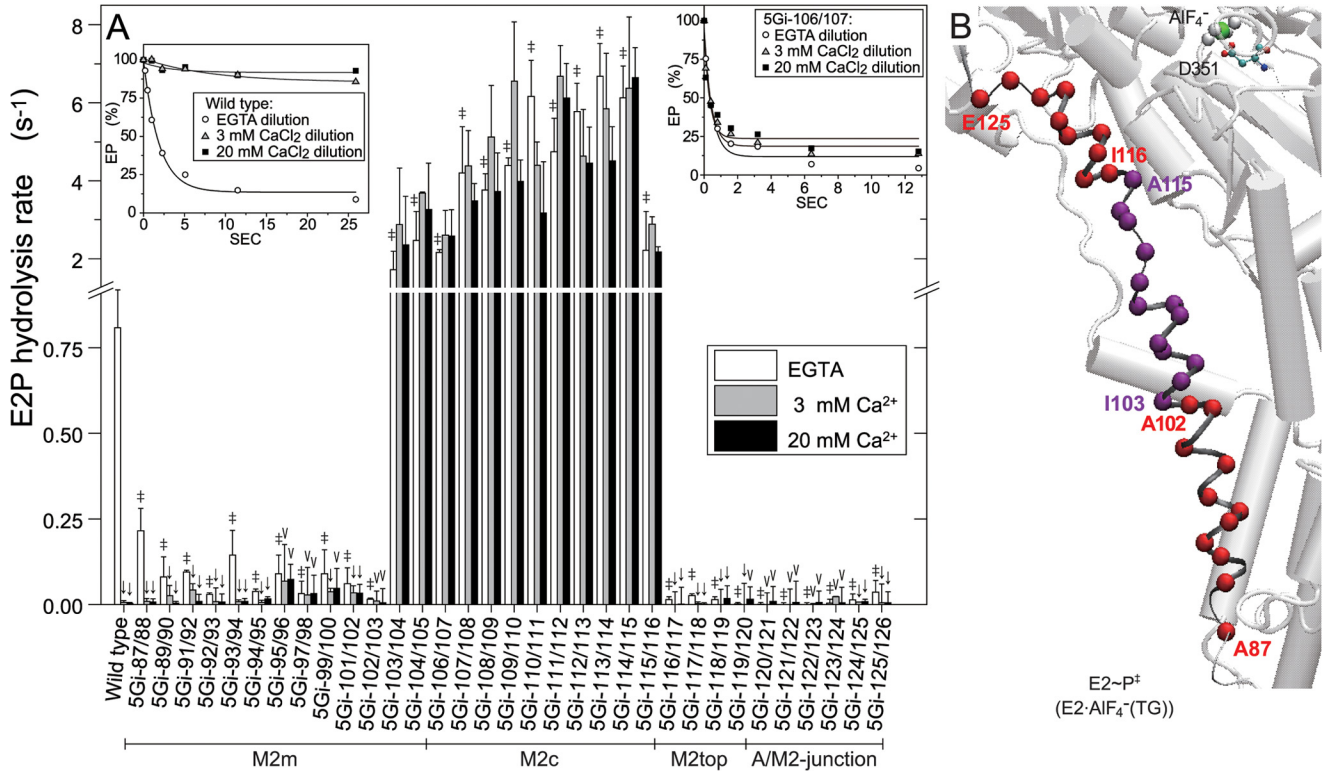

FIGURE 7. ***E2P* hydrolysis and luminal Ca^{2+}-induced inhibition.** *A*, microsomes expressing wild type or mutant were phosphorylated with $^{32}P_i$ at 25 °C for 10 min in 5 μl of a mixture containing 1–5 μg of microsomal protein, 0.1 mM $^{32}P_i$, 1 μM A23187, 0.2 mM EGTA, 7 mM $MgCl_2$, 50 mM MOPS/Tris (pH 7.0), and 35% (v/v) Me_2SO. The mixture was then cooled and diluted at 0 °C by the addition of 95 μl of a mixture containing 2.1 mM non-radioactive P_i, 105 mM KCl, 7 mM $MgCl_2$, 50 mM MOPS/Tris (pH 7.0), and 3 mM EGTA (*open bar*) or 3.2 mM (*gray bar*) and 21.1 mM (*closed bar*) $CaCl_2$ in place of EGTA, and *E*2P hydrolysis was followed (see typical examples with wild type and 5Gi-106/107 in the *inset*). The amounts of *E*2P formed with $^{32}P_i$ at zero time are normalized to 100%. *Solid lines* show the least squares fit to a single exponential, and the rates thus obtained are shown in the *main panel*. In the absence of Ca^{2+}, statistical significance of the mutant rate compared with the wild-type rate is shown above an *open bar*: *, $p < 0.05$; ‡, $p < 0.01$. In each of the mutants and the wild type, statistical significance of the rate in 3 and 20 mM Ca^{2+} compared with that in the absence of Ca^{2+} is shown above a *gray bar* and *closed bar*: *V*, $p < 0.05$; ↓, $p < 0.01$. *B*, the marked retardation and acceleration in the absence of Ca^{2+} (*open bars* in *A*) are visualized with α-carbon *coloring*, *red* and *purple*, respectively. *Error bars*, S.D.

isomerized first to a transient *E*1 state (ready to accept Ca^{2+}) with an open cytoplasmic gate and a high Ca^{2+} affinity (*E*2 → *E*1 transition; Fig. 1). Here we measured possible effects of 5Gi mutations on the transition itself (Fig. 8) as well as the affinity of the Ca^{2+} binding sites (Fig. 9).

The rate of the transition can be quantified by measuring the rate of phosphoenzyme formation following the addition of Ca^{2+} plus ATP to Ca^{2+}-deprived Ca^{2+}-ATPase. The assay takes advantage of the fact that subsequent steps (Ca^{2+} binding, ATP binding, and phosphorylation) are relatively fast. The transition is pH-sensitive, and we have found that pH 7.0 is ideal for studying the effect of mutations because, even in wild-type, at lower pH, the rate is rather slow, and at higher values, it approaches that of the subsequent steps, notably the rate of phosphorylation of Ca^{2+}-bound Ca^{2+}-ATPase (data at pH 7.0 shown in Fig. 8; other data not shown).

First, the rate of phosphorylation of Ca^{2+}-bound Ca^{2+}-ATPase *E*1Ca_2 is only marginally affected by the mutations, although the change 5Gi-89/90 is not without consequences. The transition itself is markedly slowed by 5Gi insertions in most of M2 aa 94–119 (from the upper half of M2m to M2top).

5Gi insertions higher up at the A/M2-junction (aa 120–126) are less inhibitory, and effects diminish closer to the A domain. At the luminal end of M2, mutations are without effect, except for 5Gi-89/90 and 5Gi-87/88, which have unexpected and contrary effects. In general then, most mutations in M2 affect the transition.

Possible changes in Ca^{2+}-binding properties were assessed by measuring the Ca^{2+} dependence of phosphorylation. Apparent K_d values increase somewhat (up to 5-fold) (Fig. 9) yet still remain in the high affinity (1–1.5 μM) range. The Hill coefficients hover around the usual 2. Evidently, M2 has little to do with cytoplasmic Ca^{2+} binding itself, consistent with the fact that the Ca^{2+} binding sites consist of M4, M5, M6, and M8 (Fig. 1).

DISCUSSION

We find that almost the entire M2 section plays a crucial role in coupling movements of the A domain and catalysis with gating at the transport sites. Although 5Gi insertions in border regions of the M2 sections mostly exhibit mixed kinetic properties, in general, two main regions can be distinguished: namely that in the middle (M2c), where the long M2 helix breaks during *E*2P hydrolysis, and that on either side (M2m, M2top, and A/M2-junction). Our results show that the former controls luminal gating, whereas the latter controls cytoplasm gating. In addition, insertions in part of M2m (aa 94–103) have mixed kinetic effects, probably reflecting its structural role in the M1/M2 V-shaped body and involvement in gating on both sides of the membrane with long range effects on the catalytic

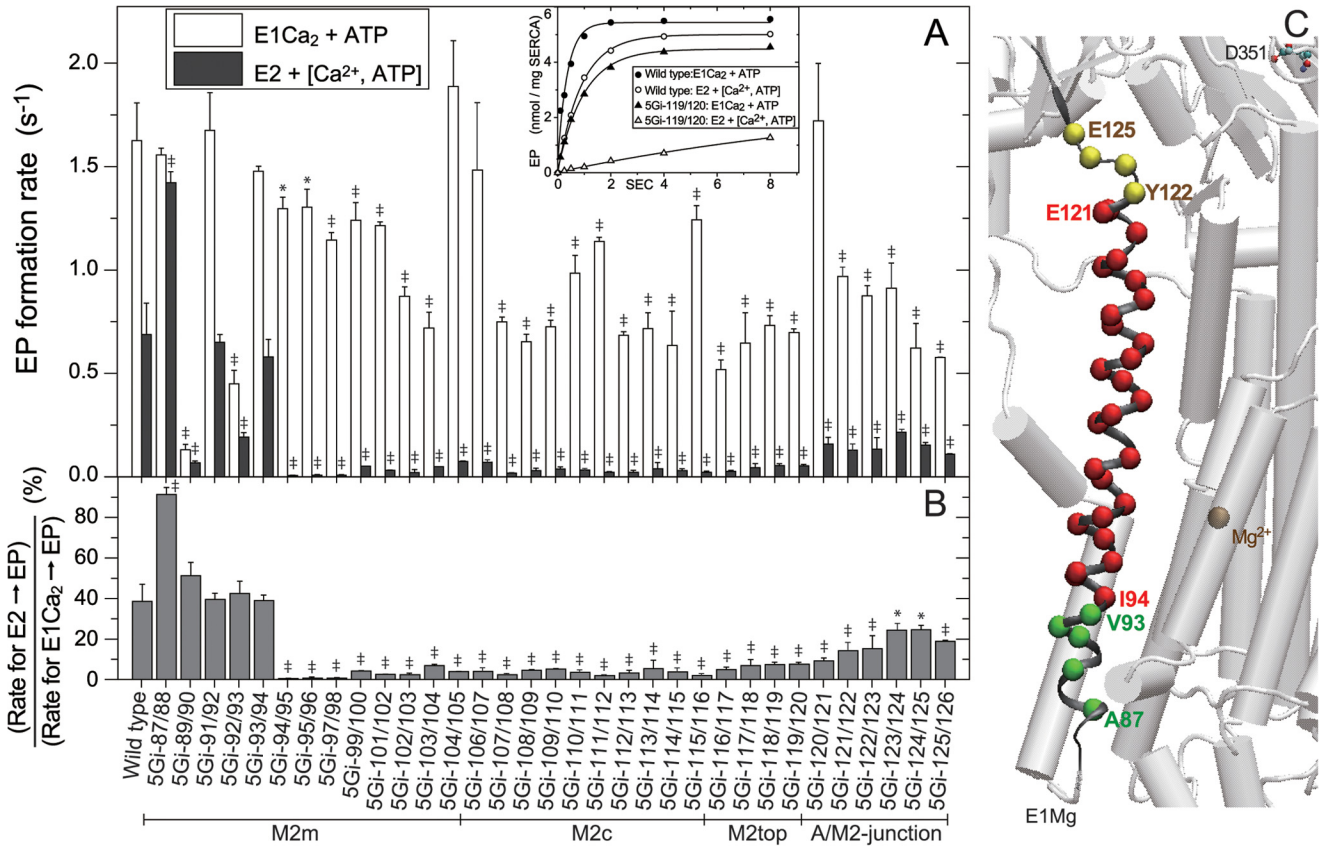

FIGURE 8. ***EP* formation from *E*2 and *E*1Ca_2 states.** *A*, microsomes expressing wild type or mutant were preincubated for 20 min at 25 °C in 50 μl of a mixture containing 1–5 μg of microsomal protein, 1 μM A23187, 0.1 M KCl, 7 mM $MgCl_2$, 50 mM MOPS/Tris (pH 7.0), and 1 mM EGTA with and without 1.2 mM $CaCl_2$ (to form the Ca^{2+}-bound (*open bar*) and unbound (*closed bar*) states, respectively). After cooling, an equal volume of a phosphorylation mixture containing 10 μM [γ-^{32}P]ATP and 1 mM EGTA with 1.2 or 2.4 mM $CaCl_2$ (to give 0.2 mM Ca^{2+} for both Ca^{2+}-bound and Ca^{2+}-unbound states) (otherwise as above) was added at 0 °C, and the *EP* formation time course was followed. In the *inset*, typical examples with the wild type and mutant 5Gi-119/120 are shown. *Solid lines* show the least squares fit to a single exponential, and the rates thus determined are shown in the *main panel*. The Ca^{2+}-unbound state was denoted as *E*2 for simplicity, and the ratio of the two rates is shown in *B*. In *A* and *B*, statistical significance compared with the respective wild-type value is shown: *, $p < 0.05$; ‡, $p < 0.01$. *C*, the observed effects on the rate-limiting process *E*2 → *E*1 in *B* are visualized with α-carbon coloring; *green*, no effect or acceleration (ratio higher than 35%); *yellow*, retardation (ratio 30–15%); *red*, marked retardation (ratio lower than 15%). *Error bars*, S.D.

site (9, 11). The results are best interpreted with reference to Fig. 10.

Cytoplasmic Gating in E2 → E1—Opening of the cytoplasm gate takes place during the *E*2 → *E*1 transition. Our results show that 5Gi insertions along most of M2 (aa 94–119) markedly retard this transition, indicating the critical importance of the helix structure for a rapid transition. Consistently, the relevant crystal structures show that the unwound Asn^{111}–Asn^{115} part of M2c in *E*2 is rewound in *E*1Mg^{2+}, a change associated with the ~110° A domain rotation (14), and M2 becomes a contiguous helix in *E*1Mg^{2+}, as in *E*1Ca_2. In the critical region aa 94–119, the lower half (aa 94–111) and the upper half (aa 111–119) change from broken and disengaged entities in *E*2 to making strong helix-helix contacts with M6 and M4C in *E*1, respectively (*gray circle* and *yellow circle* in *panel b* in Fig. 10*A*). These helix-helix interactions probably must stabilize the *E*1 structure, facilitating the *E*2 → *E*1 transition and opening of the cytoplasmic gate.

Cytoplasmic Gating in E1P and Its Isomerization—Once the two Ca^{2+} bind to the transport sites from the cytoplasmic side, closing of the gate to occlude the Ca^{2+} is effected by phosphorylation to *E*1P (9, 43, 44). Two sets of mutations, those in M2m and those in the M2top~A/M2-junction, but not in the middle at M2c, uncouple the pump and fail to occlude Ca^{2+}, indicating the importance of these regions in stabilizing the closed cytoplasmic gate.

The immediate gating residue is Glu^{309}, and Leu^{65} in M1 fastens it down as demonstrated previously (9, 43, 44). As seen (*gray circle* in *panel d* in Fig. 10*B*), the region around Leu^{98} in M2m is in close contact with Leu^{65} by hydrophobic interactions producing the M1/M2 V-shaped body and also directly with Glu^{309}. The disruption of the hydrophobic Leu^{98} region probably allowed greater freedom of movement of Glu^{309}, thereby permitting the Ca^{2+} to escape. It is also possible that luminal gate opening is also impaired because *E*P isomerization and opening depends on the motion of the M1/M2 V-shaped body, which is formed by the interactions of the hydrophobic Leu^{98} region with M1 (11).

In mutants at the A/M2-junction and M2top, we did not observe Ca^{2+} occlusion because of the low level of *E*1P (Figs. 5 and 6), but it is evident from the lack of transport that Ca^{2+} escaped from the transport sites either in *E*1P or during the isomerization to *E*2P. A properly stabilized M2 and A domain must be critical for maintaining a closed cytoplasmic gate. Interestingly, the severe uncoupling is accompanied by acceleration of *E*P isomerization. It is as if freedom from coupling

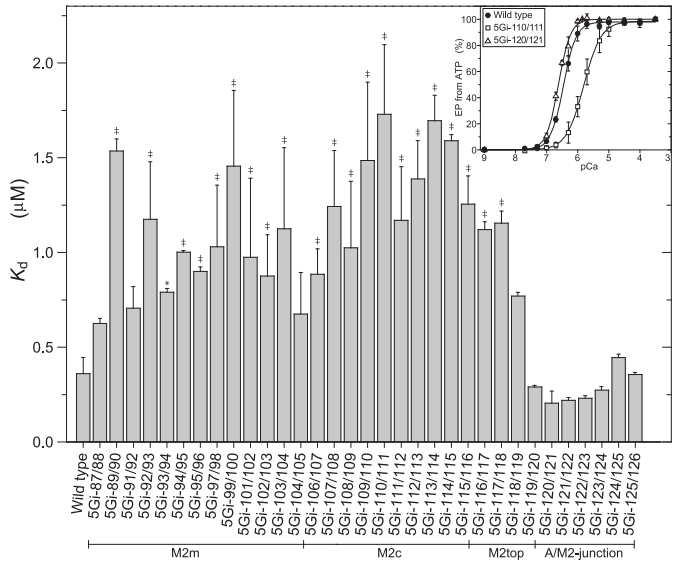

FIGURE 9. **Ca^{2+} affinity determined with *EP* formation.** The microsomes expressing wild type or mutant were preincubated for 20 min at 25 °C in 45 μl of a mixture containing 1–5 μg of microsomal protein, 2 mM EGTA, 1 μM A23187, 0.1 M KCl, 7 mM $MgCl_2$, 50 mM MOPS/Tris (pH 7.0), and various concentrations of $CaCl_2$ to give the desired Ca^{2+} concentrations. After cooling, the Ca^{2+}-ATPase was phosphorylated with 10 μM [γ-^{32}P]ATP for 15 s at 0 °C, and the amount of *EP* formed was determined. In the *inset*, the typical Ca^{2+} dependence of *EP* formation was shown for the wild type and the two mutants including 5Gi-110/111, which gave the highest K_d value. The K_d value and Hill coefficient were estimated by least squares fit to the Hill equation (*solid line*). The Hill coefficient obtained was ~2 (actually 1.6–2) in the wild type and all of the mutants. Statistical significance compared with the wild type is shown: *, $p < 0.05$; ‡, $p < 0.01$. *Error bars*, S.D.

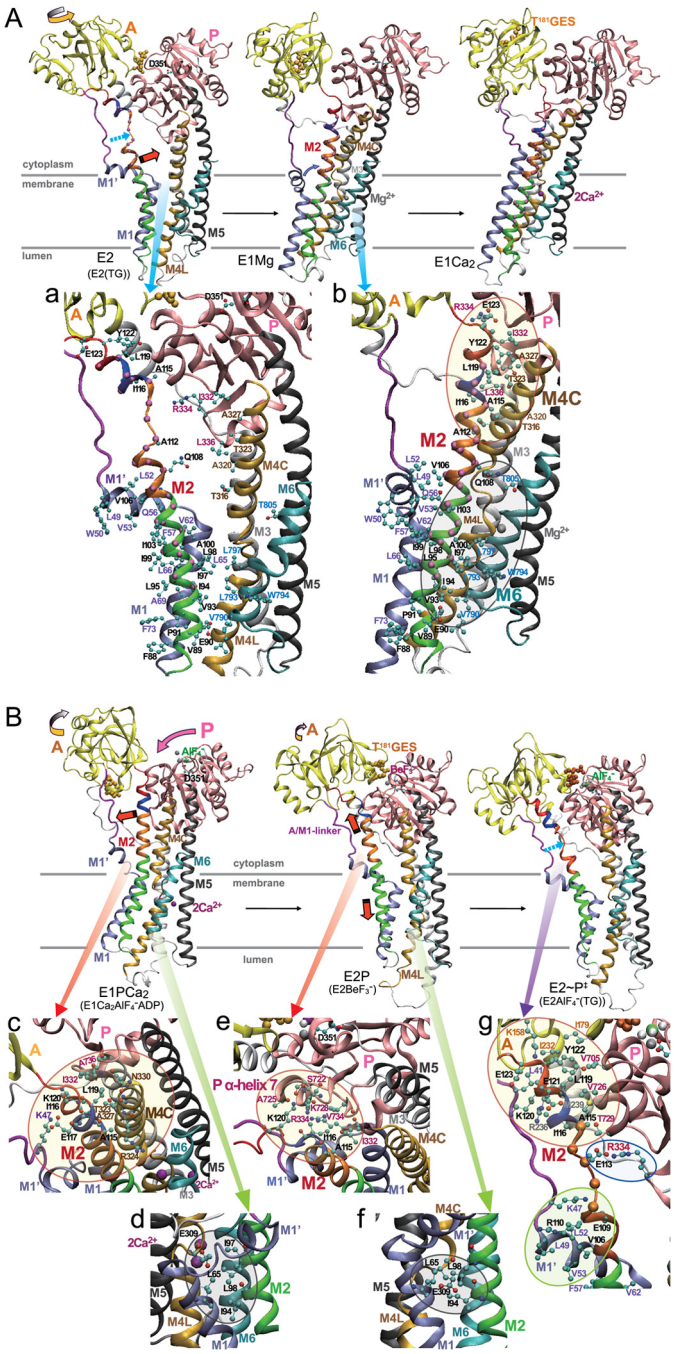

FIGURE 10. **Detailed inspection of structure and interactions of M2 in crystal structures.** The structural changes are modeled as in Fig. 1*A*. The N domain and M7–M10 helices are not depicted for simplicity. The *red* (*A* and *B*), *ice blue* (*A*), *yellow* (*A* and *B*), and *pink* (*B*) *arrows* indicate the approximate motions of M2, M1′, A domain, and P domain, respectively. The *broken light blue arrow* (*A* and *B*) indicates the unwound part of M2. The TGES^{184} loop is depicted with *orange van der Waals spheres*. Interactions involving M2 regions are shown in *transparent circles* in *enlarged views*. See "Discussion" for the details and the roles of M2 regions.

rechannels the energy into a faster transition. The extensive slack caused by the 5Gi insertions evidently uncoupled and accelerated *E*1P → *E*2P. In the change, $E1Ca_2{\cdot}AlF_4^-{\cdot}ADP \rightarrow E2{\cdot}BeF_3^-$, the A/M2-junction~M2top loop region does indeed seem to be strained, because, for example, the distance between Glu^{117}-αC and Glu^{125}-αC increases from 14.3 Å in $E1Ca_2{\cdot}AlF_4^-{\cdot}ADP$ (PDB code 1T5T) to 15.7 or 17.3 Å in $E2{\cdot}BeF_3^-$ (PDB code 2ZBE or 3B9B), thus by 1.4 or 3.0 Å.

The closer the M2top mutations get to the A/M2-junction the more severe the uncoupling, suggesting that M2top stabilizes the junction and a closed Glu^{309} gate. The M2top mutations also strongly accelerate *EP* isomerization; therefore, in the wild type, there must be some structural restriction here. Indeed, in the crystal structure of *E*1P ($E1Ca_2{\cdot}AlF_4^-{\cdot}ADP$), M2top interacts with the cytoplasmic half of M4 (M4C, *yellow circle* in *panel c* in Fig. 10*B*), and in *E*2P ($E2{\cdot}BeF_3^-$), it interacts with the bottom of the P domain and α-helix 7 (*yellow circle* in *panel e* in Fig. 10*B*).

A mechanistic scenario for the *EP* isomerization and gating with respect to the A/M-junction~M2top may be as follows. During the *E*1P → *E*2P isomerization, the A domain rotates and pulls on A/M2-junction~M2top, straining it to detach from M4C. The P domain/M4/M5 entity is now able to incline toward the underside of the A domain to produce new interactions with M2top (Fig. 10*B*). In these coupled motions, the M1/M2 V-shaped body and M4/M5 probably move coordinately, keeping the Glu^{309} gate closed. Kinetically, coupling and proper Ca^{2+} handling have an energy cost: the rate-limiting slow *EP* isomerization. Ca^{2+} deocclusion and release from $E2PCa_2$ involves further inclination of the A and P domains due to strain in the A/M1′-linker, with the A domain lodging above the P domain in $E2PCa_2$, and the luminal gate opens to release Ca^{2+} (24, 25). Thus, the A domain's M2 link and A/M1′-linker have distinct functions; the former keeps the cytoplasmic gate closed, and the latter is needed for opening the luminal gate, both regions coupling A domain motions with gating.

The importance of an intact A/M2-junction∼M2top interaction is further underpinned by the fact that mutations in the M2c region do not have the same deleterious effects (uncoupling with accelerated *E*P isomerization) because the interactions of M2top with the M4C/P-domain and of M2m (M1/M2 V-shaped body) to fix the Glu^{309} gate are normal in these mutants. Also, M2c does not interact strongly with other parts both in *E*1P and *E*2P and does not change structure (is not strained) during the *E*P isomerization. The mutations here are silent. Also, as noted above, the A domain motion driving Ca^{2+} release into the lumen after the *E*P isomerization is controlled to a significant extent by the A/M1′-linker, another cytoplasmic link (24, 25), and evidently not by M2c.

Luminal Gating—Opening of the luminal gate and Ca^{2+} release is effected during $E1P \rightarrow E2P$, and the latter Ca^{2+}-free state becomes susceptible to Ca^{2+} binding from the lumen at high Ca^{2+} concentrations (back-inhibition). The gate closes during *E*2P hydrolysis $E2P \rightarrow E2{\sim}P^{\ddagger}$ with most of Ca^{2+}-binding residues protonated, according to both biochemical evidence (7) and relevant crystal structures (9, 11, 12).

We find that *E*2P hydrolysis is markedly accelerated by 5Gi insertions at aa 103–115 in the M2c region, in sharp contrast to the marked retardation by those at adjacent regions aa 87–102 on M2m and aa 116–125 on M2top∼A/M2-junction (Fig. 7). Significantly, acceleration is accompanied by the almost complete resistance against inhibition by luminal Ca^{2+} even up to 20 mM. Most of these mutants (aa 106–115) are well coupled in terms of Ca^{2+} transport/ATP hydrolysis ratios. Therefore, Ca^{2+} must be released to the lumen, but the binding sites are unavailable for Ca^{2+} rebinding from the lumen due to the rapid *E*2P hydrolysis and closure of the luminal gate. Alternatively, luminal Ca^{2+} binding is no longer coupled to a large change in the rate of hydrolysis.

The results indicate that a proper unwinding/elongation on M2c with properly controlled *E*2P hydrolysis may be critical for coupling the change in $E2P \rightarrow E2{\sim}P^{\ddagger}$ at the catalytic site with the luminal gate closure. The 5Gi insertions exaggerated both coupled structural events. Physiologically, the setting of the luminal Ca^{2+} concentration is governed by the Ca^{2+}-induced back-inhibition of *E*2P hydrolysis (22, 24, 37–42, 45). In the wild type, the regionally limited partial unwinding/elongation in M2c appears critical for the set point, but it comes with an energy cost: slow but properly controlled gate closing coupled to *E*2P hydrolysis.

Then, in the structural change mimicking $E2P \rightarrow E2{\sim}P^{\ddagger}$ (Fig. 10*B*), a part of helical M2c, Asn^{111}–Ala^{115}, unwinds and extends 7 Å, which is due to strain exerted through a 25° rotation of the A domain upon water attack at the active site to effect hydrolysis (11). Thereby, the lower part of M2 moves downward 6 Å, inclines, and presses the M1/M2 V-shaped rigid body on M3 and M4 to close the luminal gate (11). In $E2{\sim}P^{\ddagger}$, the interactions between M2c and the rest of the protein are rather weak, whereas those between the regions on either side and protein are helix to helix, extensive, and therefore fixed (*yellow* and *green circles* in *panel g* in Fig. 10*B*). Thus, it appears that M2 is literally pulled apart at M2c. Evidently, the 5Gi mutations in this weak region facilitate and exaggerate (possibly causing elongation of up to ∼17 Å) these processes, resulting in an activation of hydrolysis and fast and tight closure of the transport sites (or uncoupling). Consistently, mutations that disrupt the strong helix to helix interactions at the bottom of M2c (aa 103–110) with the M1′ helix alongside resulted in accelerated and luminal Ca^{2+}-resistant *E*2P hydrolysis.

In contrast, mutations higher up, in the M2top∼A/M2-junction, impede hydrolysis and closure, probably by affecting interactions with the A and P domains and the Tyr^{122}-hydrophobic cluster, which was previously demonstrated to be critical for proper catalytic site formation in *E*2P with hydrolytic ability (*yellow circle* in *panel g* in Fig. 10*B*) (21, 22, 46). Mutations lower down, in aa 87–102 of M2m, disrupt arrangement of the transmembrane helices and probably cause a long range effect on the A and P domain interaction and catalytic site, thus retarding *E*2P hydrolysis. Note that mutants at the region aa 95–101 showed some resistance against luminal Ca^{2+}-induced back-inhibition. This region forms the M1/M2 V-shaped body, and the downward movement of M2 with inclination of the body is critical for the luminal gate closure (9, 11). The 5Gi elongation in this region probably exaggerated such motions and tightened gate closure.

The long M2 helix and probably the A domain's motion are common structural features in P-type ion-pumping ATPases (16–20). The strategy employed here of systematically introducing 5Gi insertions along M2 to disrupt the helix and relieve strain may be helpful for exploring the role of M2 in coupling A domain movements with gating and catalysis in other P-type ATPases.

Acknowledgments—We thank Dr. David H. MacLennan (University of Toronto) for the generous gift of SERCA1a cDNA and Dr. Randal J. Kaufman (Genetics Institute, Cambridge, MA) for the generous gift of the expression vector pMT2. We are also grateful to Dr. Chikashi Toyoshima (University of Tokyo) for helpful discussions. We thank Dr. Yasuaki Saijo (Asahikawa Medical University) for assistance in statistical analysis and Dr. David B. McIntosh for reviewing and improving the manuscript.

REFERENCES

1. Toyoshima, C. (2008) Structural aspects of ion pumping by Ca^{2+}-ATPase of sarcoplasmic reticulum. *Arch. Biochem. Biophys.* **476,** 3–11
2. Toyoshima, C. (2009) How Ca^{2+}-ATPase pumps ions across the sarcoplasmic reticulum membrane. *Biochim. Biophys. Acta* **1793,** 941–946
3. Møller, J. V., Olesen, C., Winther, A.-M. L., and Nissen, P. (2010) The sarcoplasmic Ca^{2+}-ATPase: design of a perfect chemi-osmotic pump. *Q. Rev. Biophys.* **43,** 501–566
4. Toyoshima, C., Nakasako, M., Nomura, H., and Ogawa, H. (2000) Crystal structure of the calcium pump of sarcoplasmic reticulum at 2.6 Å resolution. *Nature* **405,** 647–655
5. Danko, S., Yamasaki, K., Daiho, T., Suzuki, H., and Toyoshima, C. (2001) Organization of cytoplasmic domains of sarcoplasmic reticulum Ca^{2+}-ATPase in E_1P and E_1ATP states: a limited proteolysis study. *FEBS Lett.* **505,** 129–135
6. Toyoshima, C., and Nomura, H. (2002) Structural changes in the calcium pump accompanying the dissociation of calcium. *Nature* **418,** 605–611
7. Danko, S., Yamasaki, K., Daiho, T., and Suzuki, H. (2004) Distinct natures of beryllium fluoride-bound, aluminum fluoride-bound, and magnesium fluoride-bound stable analogues of an ADP-insensitive phosphoenzyme intermediate of sarcoplasmic reticulum Ca^{2+}-ATPase. *J. Biol. Chem.* **279,** 14991–14998
8. Toyoshima, C., and Mizutani, T. (2004) Crystal structure of the calcium

pump with a bound ATP analogue. *Nature* **430,** 529–535
9. Toyoshima, C., Nomura, H., and Tsuda, T. (2004) Lumenal gating mechanism revealed in calcium pump crystal structures with phosphate analogues. *Nature* **432,** 361–368
10. Sørensen, T. L.-M., Møller, J. V., and Nissen, P. (2004) Phosphoryl transfer and calcium ion occlusion in the calcium pump. *Science* **304,** 1672–1675
11. Toyoshima, C., Norimatsu, Y., Iwasawa, S., Tsuda, T., and Ogawa, H. (2007) How processing of aspartylphosphate is coupled to lumenal gating of the ion pathway in the calcium pump. *Proc. Natl. Acad. Sci. U.S.A.* **104,** 19831–19836
12. Olesen, C., Picard, M., Winther, A. M., Gyrup, C., Morth, J. P., Oxvig, C., Møller, J. V., and Nissen, P. (2007) The structural basis of calcium transport by the calcium pump. *Nature* **450,** 1036–1042
13. Danko, S., Daiho, T., Yamasaki, K., Liu, X., and Suzuki, H. (2009) Formation of the stable structural analog of ADP-sensitive phosphoenzyme of Ca^{2+}-ATPase with occluded Ca^{2+} by beryllium fluoride. *J. Biol. Chem.* **284,** 22722–22735
14. Toyoshima, C., Iwasawa, S., Ogawa, H., Hirata, A., Tsueda, J., and Inesi, G. (2013) Crystal structures of the calcium pump and sarcolipin in the Mg^{2+}-bound E1 state. *Nature* **495,** 260–264
15. Winther, A. M., Bublitz, M., Karlsen, J. L., Møller, J. V., Hansen, J. B., Nissen, P., and Buch-Pedersen, M. J. (2013) The sarcolipin-bound calcium pump stabilizes calcium sites exposed to the cytoplasm. *Nature* **495,** 265–269
16. Toyoshima, C., and Inesi, G. (2004) Structural basis of ion pumping by Ca^{2+}-ATPase of the sarcoplasmic reticulum. *Annu. Rev. Biochem.* **73,** 269–292
17. Kanai, R., Ogawa, H., Vilsen, B., Cornelius, F., and Toyoshima, C. (2013) Crystal structure of a Na^+-bound Na^+,K^+-ATPase preceding the E1P state. *Nature* **502,** 201–206
18. Shinoda, T., Ogawa, H., Cornelius, F., and Toyoshima, C. (2009) Crystal structure of the sodium-potassium pump at 2.4 Å resolution. *Nature* **459,** 446–450
19. Abe, K., Tani, K., and Fujiyoshi, Y. (2011) Conformational rearrangement of gastric H^+,K^+-ATPase induced by an acid suppressant. *Nat. Commun.* **2,** 155
20. Bublitz, M., Poulsen, H., Morth, J. P., and Nissen, P. (2010) In and out of the cation pumps: P-type ATPase structure revisited. *Curr. Opin. Struct. Biol.* **20,** 431–439
21. Wang, G., Yamasaki, K., Daiho, T., and Suzuki, H. (2005) Critical hydrophobic interactions between phosphorylation and actuator domains of Ca^{2+}-ATPase for hydrolysis of phosphorylated intermediate. *J. Biol. Chem.* **280,** 26508–26516
22. Yamasaki, K., Wang, G., Daiho, T., Danko, S., and Suzuki, H. (2008) Roles of Tyr^{122}-hydrophobic cluster and K^+ binding in Ca^{2+}-releasing process of ADP-insensitive phosphoenzyme of sarcoplasmic reticulum Ca^{2+}-ATPase. *J. Biol. Chem.* **283,** 29144–29155
23. Daiho, T., Yamasaki, K., Wang, G., Danko, S., Iizuka, H., and Suzuki, H. (2003) Deletions of any single residues in Glu^{40}–Ser^{48} loop connecting A domain and the first transmembrane helix of sarcoplasmic reticulum Ca^{2+}-ATPase result in almost complete inhibition of conformational transition and hydrolysis of phosphoenzyme intermediate. *J. Biol. Chem.* **278,** 39197–39204
24. Daiho, T., Yamasaki, K., Danko, S., and Suzuki, H. (2007) Critical role of Glu^{40}–Ser^{48} loop linking actuator domain and first transmembrane helix of Ca^{2+}-ATPase in Ca^{2+} deocclusion and release from ADP-insensitive phosphoenzyme. *J. Biol. Chem.* **282,** 34429–34447
25. Daiho, T., Danko, S., Yamasaki, K., and Suzuki, H. (2010) Stable structural analog of Ca^{2+}-ATPase ADP-insensitive phosphoenzyme with occluded Ca^{2+} formed by elongation of A-domain/M1′-linker and beryllium fluoride binding. *J. Biol. Chem.* **285,** 24538–24547
26. Kaufman, R. J., Davies, M. V., Pathak, V. K., and Hershey, J. W. (1989) The phosphorylation state of eucaryotic initiation factor 2 alters translational efficiency of specific mRNAs. *Mol. Cell Biol.* **9,** 946–958
27. Maruyama, K., and MacLennan, D. H. (1988) Mutation of aspartic acid-351, lysine-352, and lysine-515 alters the Ca^{2+} transport activity of the Ca^{2+}-ATPase expressed in COS-1 cells. *Proc. Natl. Acad. Sci. U.S.A.* **85,** 3314–3318
28. Daiho, T., Yamasaki, K., Suzuki, H., Saino, T., and Kanazawa, T. (1999) Deletions or specific substitutions of a few residues in the NH_2-terminal region (Ala^3 to Thr^9) of sarcoplasmic reticulum Ca^{2+}-ATPase cause inactivation and rapid degradation of the enzyme expressed in COS-1 cells. *J. Biol. Chem.* **274,** 23910–23915
29. Daiho, T., Yamasaki, K., Saino, T., Kamidochi, M., Satoh, K., Iizuka, H., and Suzuki, H. (2001) Mutations of either or both Cys^{876} and Cys^{888} residues of sarcoplasmic reticulum Ca^{2+}-ATPase result in a complete loss of Ca^{2+} transport activity without a loss of Ca^{2+}-dependent ATPase activity: Role of the Cys^{876}-Cys^{888} Disulfide Bond. *J. Biol. Chem.* **276,** 32771–32778
30. Weber, K., and Osborn, M. (1969) The reliability of molecular weight determinations by dodecyl sulfate-polyacrylamide gel electrophoresis. *J. Biol. Chem.* **244,** 4406–4412
31. Daiho, T., Suzuki, H., Yamasaki, K., Saino, T., and Kanazawa, T. (1999) Mutations of Arg^{198} in sarcoplasmic reticulum Ca^{2+}-ATPase cause inhibition of hydrolysis of the phosphoenzyme intermediate formed from inorganic phosphate. *FEBS Lett.* **444,** 54–58
32. Lowry, O. H., Rosebrough, N. J., Farr, A. L., and Randall, R. J. (1951) Protein measurement with the folin phenol reagent. *J. Biol. Chem.* **193,** 265–275
33. Humphrey, W., Dalke, A., and Schulten, K. (1996) VMD: visual molecular dynamics. *J. Mol. Graph.* **14,** 33–38, 27–28
34. Sagara, Y., and Inesi, G. (1991) Inhibition of the sarcoplasmic reticulum Ca^{2+} transport ATPase by thapsigargin at subnanomolar concentrations. *J. Biol. Chem.* **266,** 13503–13506
35. Shigekawa, M., and Dougherty, J. P. (1978) Reaction mechanism of Ca^{2+}-dependent ATP hydrolysis by skeletal muscle sarcoplasmic reticulum in the absence of added alkali metal salts. II. Kinetic properties of the phosphoenzyme formed at the steady state in high Mg^{2+} and low Ca^{2+} concentrations. *J. Biol. Chem.* **253,** 1451–1457
36. de Meis, L., Martins, O. B., and Alves, E. W. (1980) Role of water, hydrogen ion, and temperature on the synthesis of adenosine triphosphate by the sarcoplasmic reticulum adenosine triphosphatase in the absence of a calcium ion gradient. *Biochemistry* **19,** 4252–4261
37. Sato, K., Yamasaki, K., Daiho, T., Miyauchi, Y., Takahashi, H., Ishida-Yamamoto, A., Nakamura, S., Iizuka, H., and Suzuki, H. (2004) Distinct types of abnormality in kinetic properties of three Darier disease-causing sarco(endo)plasmic reticulum Ca^{2+}-ATPase mutants that exhibit normal expression and high Ca^{2+} transport activity. *J. Biol. Chem.* **279,** 35595–35603
38. de Meis, L., and Inesi, G. (1982) ATP synthesis by sarcoplasmic reticulum ATPase following Ca^{2+}, PH, temperature, and water activity jumps. *J. Biol. Chem.* **257,** 1289–1294
39. Nakamura, Y. (1984) Two alternate kinetic routes for the decomposition of the phosphorylated intermediate of sarcoplasmic reticulum Ca^{2+}-ATPase. *J. Biol. Chem.* **259,** 8183–8189
40. Nakamura, Y., Kurzmack, M., and Inesi, G. (1986) Kinetic effects of calcium and ADP on the phosphorylated intermediate of sarcoplasmic reticulum ATPase. *J. Biol. Chem.* **261,** 3090–3097
41. Prager, R., Punzengruber, C., Kolassa, N., Winkler, F., and Suko, J. (1979) Ionized and bound calcium inside isolated sarcoplasmic reticulum of skeletal muscle and its significance in phosphorylation of adenosine triphosphatase by orthophosphate. *Eur. J. Biochem.* **97,** 239–250
42. Hanel, A. M., and Jencks, W. P. (1991) Dissociation of calcium from the phosphorylated calcium-transporting adenosine triphosphatase of sarcoplasmic reticulum: kinetic equivalence of the calcium ions bound to the phosphorylated enzyme. *Biochemistry* **30,** 11320–11330
43. Einholm, A. P., Vilsen, B., and Andersen, J. P. (2004) Importance of transmembrane segment M1 of the sarcoplasmic reticulum Ca^{2+}-ATPase in Ca^{2+} occlusion and phosphoenzyme processing. *J. Biol. Chem.* **279,** 15888–15896
44. Inesi, G., Ma, H., Lewis, D., and Xu, C. (2004) Ca^{2+} occlusion and gating function of Glu^{309} in the ADP-fluoroaluminate analog of the Ca^{2+}-ATPase phosphoenzyme intermediate. *J. Biol. Chem.* **279,** 31629–31637
45. Meldolesi, J., and Pozzan, T. (1998) The endoplasmic reticulum Ca^{2+} store: a view from the lumen. *Trends Biochem. Sci.* **23,** 10–14
46. Yamasaki, K., Daiho, T., Danko, S., and Suzuki, H. (2004) Multiple and distinct effects of mutations of Tyr^{122}, Glu^{123}, Arg^{324}, and Arg^{334} involved

in interactions between the top part of second and fourth transmembrane helices in sarcoplasmic reticulum Ca^{2+}-ATPase. *J. Biol. Chem.* **279,** 2202–2210
47. Lytton, J., Westlin, M., and Hanley, M. R. (1991) Thapsigargin inhibits the sarcoplasmic or endoplasmic reticulum Ca-ATPase family of calcium pumps. *J. Biol. Chem.* **266,** 17067–17071
48. Garnett, C., Sumbilla, C., Belda, F. F., Chen, L., and Inesi, G. (1996) Energy transduction and kinetic regulation by the peptide segment connecting phosphorylation and cation binding domains in transport ATPases. *Biochemistry* **35,** 11019–11025
49. Xu, C., Prasad, A. M., Inesi, G., and Toyoshima, C. (2008) Critical role of Val-304 in conformational transitions that allow Ca^{2+} occlusion and phosphoenzyme turnover in the Ca^{2+} transport ATPase. *J. Biol. Chem.* **283,** 3297–3304